Alignments and shape changes in ^{77}Se

G. D. Johns,* J. Döring, R. A. Kaye, G. N. Sylvan, and S. L. Tabor
Department of Physics, Florida State University, Tallahassee, Florida 32306
(Received 30 September 1996)

High-spin states in ^{77}Se were studied using the ^{76}Ge(α,3n) reaction at 40 MeV at the Florida State University Tandem-LINAC facility. Prompt γ-γ coincidences were observed using the Pitt-FSU detector array. The positive- and negative-parity yrast bands were extended up to spins of $(\frac{31}{2}^+)$ and $(\frac{27}{2}^-)$, respectively. Spin assignments were made based on directional correlation of oriented nuclei ratios whenever possible. A rich and complicated high-lying high-K negative-parity structure was also found. The positive-parity yrast structure shows a change from large signature splitting at low spin to a more uniform level spacing at higher spins, as has been seen in the heavier $N=43$ isotones. Theoretically, this change is attributed to a shift from oblate to triaxial shape due to the alignment of a pair of $g_{9/2}$ protons. [S0556-2813(97)04702-X]

PACS number(s): 23.20.Lv, 25.55.−e, 27.50.+e, 29.30.Kv

I. INTRODUCTION

Nuclei in the region of deformation with neutron and proton numbers between 28 and 50 exhibit a wide range of shapes and are quite sensitive to the polarizing effects of individual nucleons. One of the best examples is the $N=43$ isotones. The valence neutron has been shown [1] to drive the shape of ^{81}Sr from oblate to moderately deformed prolate to highly deformed ($\beta_2 \sim 0.4$) prolate, depending on the orbital occupied. Additional quasiparticles (qp's) drive the nucleus to triaxial and even superdeformed [2] shapes.

A structural similarity is expected among the even-Z, odd-N isotones since the same orbitals are available to the valence neutron. This is especially clear among the $N=43$ isotones ^{81}Sr [1–4], ^{79}Kr [5–7], and ^{83}Zr [8–11]. There are similar rotational bands in these nuclei built on the $\frac{1}{2}^-$ ground state and low-lying $\frac{3}{2}^-$, $\frac{5}{2}^-$, $\frac{5}{2}^+$, $\frac{7}{2}^+$, and $\frac{11}{2}^+$ levels. The yrast band, based on a $\nu g_{9/2}$ configuration, is the most unique among these. Unlike the other bands, it shows large signature splitting up to the $\frac{21}{2}^+$ state, after which the signature splitting abruptly disappears and $\Delta I=1$ decays become strong. At even higher spins, the signature splitting gradually returns. Theoretically, the $g_{9/2}$ quasineutron polarizes the core to an oblate shape, leading to large signature splitting at low spins. After the first band crossing, two $g_{9/2}$ quasiprotons drive the nucleus to a triaxial shape and reduced signature splitting. Above this, a gradual quasineutron alignment returns the nucleus to an oblate shape with increased signature splitting.

Since the $N=43$ isotones exhibit such a close family resemblance and changing particle numbers do affect single-particle orbitals, it is instructive to explore other even-Z, $N=43$ isotones. Only limited information was available [12] concerning the next lighter $N=43$ isotone, ^{77}Se, prior to the present work, but it did suggest some similarities with the heavier isotones. In particular, strong decays were seen in a $\frac{7}{2}^+$ band, which exhibited large signature splitting, but was not observed as high as the band-crossing region. A preliminary level scheme [13] provided suggestions of a change in signature splitting around $\frac{21}{2}^+$, and a thermal neutron-capture experiment [14], as well as an (n,$n'\gamma$) measurement [15], provided more information about the low-lying, low-spin states. In addition, some lifetime information for states up to the $\frac{25}{2}^+$ level at 4626 keV using the Doppler-shift attenuation and recoil distance techniques was presented in conference proceedings [16].

Another reason to explore the structure of ^{77}Se above the band-crossing region was to look for evidence of a high-lying, high-K band. Such interesting structures have been observed in a number of odd-Z nuclei [17], but in only one odd-N case, ^{79}Kr [5]. Such a structure has not been reported in the heavier $N=43$ isotones, but ^{77}Se is a good candidate because of its proximity to ^{79}Kr.

Although it would be preferable to investigate the high-spin structure of ^{77}Se using a heavy-ion reaction which would bring in more angular momentum, it is difficult to populate this neutron-rich isotope adequately in heavy-ion reactions. Use of the (α,3n) reaction at 40 MeV provided more spin than an earlier (α,n) experiment at 14 MeV [12], but the major improvement in the present work was the use of a larger γ-detector array.

II. EXPERIMENTAL TECHNIQUES

The Florida State University Tandem-LINAC facility was used to provide the 40 MeV α beam needed to produce the ^{76}Ge(α,3n) fusion-evaporation reaction. A 0.5 mg/cm^2 thick self-supporting target enriched to 94.6% in ^{76}Ge was used in the experiment to investigate high-spin states in ^{77}Se.

The Pitt-FSU detector array [18] used in this experiment consisted of eight Compton-suppressed high-purity Ge detectors. Four of the Ge detectors were located at 90° relative to the beam axis while the remaining four detectors were placed at 145°. Energy calibrations were first determined for the 90° detectors using a ^{152}Eu source. Four strong lines in ^{77}Se at 249.7, 331.0, 848.8, and 1079.2 keV were then used to calibrate the 145° detectors and to monitor for gain shifts during the run.

*Present address: Los Alamos National Laboratory, Los Alamos, New Mexico 87545.

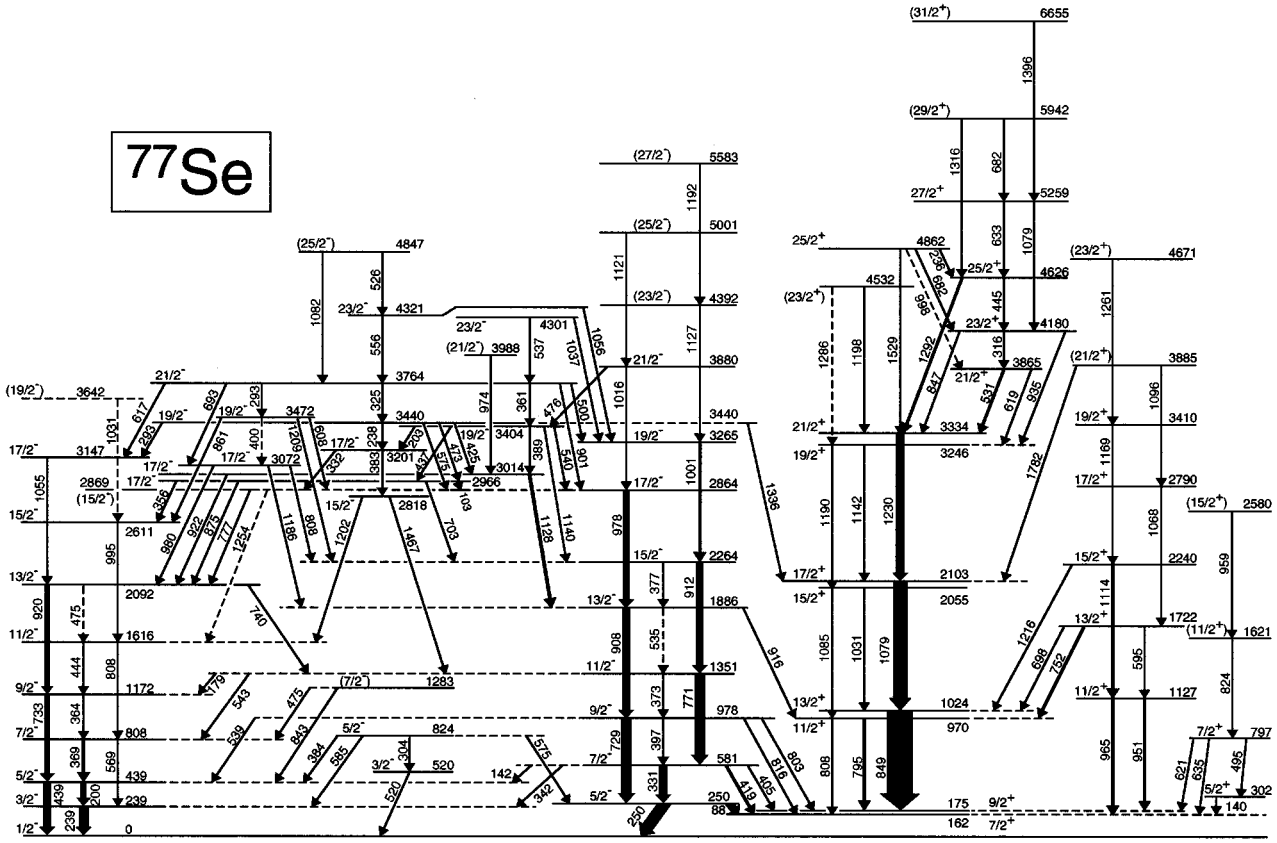

FIG. 1. The level scheme of ^{77}Se as deduced from the present work.

Approximately 15.5×10^6 γ-γ coincidences were collected and then sorted [19] into a triangular array with 2500 channels on a side with a dispersion of 0.8 keV per channel. Coincidence spectra were obtained by gating on the triangular array and subtracting a fraction of the total projection for background correction. From these gates, the coincidence relationships, γ-ray intensities, and energies were obtained and used to deduce the level scheme.

The coincidence data were also sorted into a two-dimensional square array. This array was constructed by sorting the 90° detector information onto one axis and the 145° detector information onto the other axis. Gates from this array were used to determine multipolarities of the γ-ray transitions to assist in assigning spins by extracting directional correlation of oriented nuclei (DCO) ratios whenever possible according to

$$R_{\mathrm{DCO}}=\frac{I_\gamma(\text{at } 145^\circ \text{ gated by } \gamma_G \text{ at } 90^\circ)}{I_\gamma(\text{at } 90^\circ \text{ gated by } \gamma_G \text{ at } 145^\circ)}. \qquad (1)$$

The DCO ratios for stretched electric quadrupole ($E2$) transitions are expected to have values close to 1, while $\Delta I=1$ transitions can have values ranging from 0 to 2 depending on the multipole mixing ratio δ when an $E2$ transition is used as the gating transition. If the $E2/M1$ mixing ratio is small, then the DCO ratio is expected [1] to be near 0.5. Similarly, for stretched $E1$ transitions, a DCO ratio of 0.5 is expected. If a pure $M1$ transition is used as the gate, a value of 2 is expected for stretched $E2$ transitions while a $\Delta I=1$ transition gives a value near 1 if the mixing ratio is small.

III. LEVEL SCHEME

The level scheme shown in Fig. 1 was deduced from coincidence spectra generated by gating on the triangular array. Level and transition energies, spins, relative intensities, branching ratios, and DCO ratios are given in Table I.

A. Yrast positive-parity band

The positive-parity $\alpha=\frac{1}{2}$ signature band was previously known up to the 2103 keV level [12] and has since been extended up to the 4626 keV level [13]. The present work confirms these results and has extended this band up to the $(\frac{29}{2}^+)$ 5942 keV level. The signature-partner ($\alpha=-\frac{1}{2}$) band was known up to the 3246 keV level [13]. This band has been confirmed and extended up to the $(\frac{31}{2}^+)$ 6655 keV level in the present work. A sequence of $\Delta I=1$ transitions has been added from the 3334 keV level up to the $(\frac{29}{2}^+)$ 5942 keV level.

Evidence was found for high-lying transitions close in energy to the strong 849 and 1079 keV lines. An 847 keV γ ray is clearly in coincidence with the 849 keV line, as shown in Fig. 2. Similarly, a 1079 keV line appears in the 1079 keV gated spectrum. The placement of these high-lying transitions is supported by the energy differences and the intensity patterns. For example, the 1079 keV line is considerably stronger relative to the 1230 keV γ ray in gates such as 1396 keV, which are in coincidence with both 1079 keV transitions, than in gates such as 1292 keV which exclude one 1079 keV transition. For the 847-849 keV doublet, both the intensity and the centroid are gate dependent. The place-

TABLE I. Energies, relative intensities, branching ratios (BR), and DCO ratios for transitions in ^{77}Se.

E_{lev} (keV)	E_γ (keV)	I_i^π	I_f^π	I_γ[a]	BR (%)	R_{DCO}[b]	R_{DCO}[c]
161.9	161.9223(7)[d]	$7/2^+$	$1/2^-$		100		
175.3	175.3053(15)[d]	$9/2^+$	$1/2^-$		100		
238.8	238.8(2)	$3/2^-$	$1/2^-$	33.0(10)	100	0.84(10)	
249.7	88.0(2)	$5/2^-$	$7/2^+$	43.3(10)	52(1)	0.84(12)	
	249.7(2)	$5/2^-$	$1/2^-$	40.0(10)	48(1)	0.95(12)	
301.6	139.7(4)	$5/2^+$	$7/2^+$	6.0(20)	100		1.05(20)
439.1	200.4(2)	$5/2^-$	$3/2^-$	18.3(10)	41(2)	0.63(6)	0.92(8)
	439.1(2)	$5/2^-$	$1/2^-$	26.4(10)	59(2)	0.99(6)	
520.4	520.4(3)	$3/2^-$	$1/2^-$	8.0(25)	100		
580.7	141.6(2)	$7/2^-$	$5/2^-$	1.2(6)	2(1)	0.58(10)	
	331.0(2)	$7/2^-$	$5/2^-$	35.0(10)	66(3)	1.25(8)	
	341.8(2)	$7/2^-$	$3/2^-$	3.8(9)	7(2)	1.06(16)	1.53(16)
	405.4(3)	$7/2^-$	$9/2^+$	3.8(13)	7(2)	0.64(9)	
	418.9(2)	$7/2^-$	$7/2^+$	9.2(13)	18(2)	1.07(14)	
796.5	494.7(3)	$7/2^+$	$5/2^+$	6.5(20)	42(11)		0.90(16)
	621.2(4)	$7/2^+$	$9/2^+$	5.6(20)	36(11)		
	634.6(8)	$7/2^+$	$7/2^+$	3.4(20)	22(11)		
807.9	368.6(2)	$7/2^-$	$5/2^-$	9.5(10)	54(4)	0.70(10)	1.06(8)
	569.1(3)	$7/2^-$	$3/2^-$	8.1(10)	46(4)	1.02(12)	1.57(12)
824.0	303.6(3)	$5/2^-$	$3/2^-$	0.8(4)	15(7)		
	383.8(8)	$5/2^-$	$5/2^-$	2.1(6)	40(10)	0.83(20)	
	575.0(8)	$5/2^-$	$5/2^-$	1.0(5)	19(9)		
	585.1(3)	$5/2^-$	$3/2^-$	1.3(6)	26(10)		
970.0	794.7(3)	$11/2^+$	$9/2^+$	20.0(13)	79(4)		1.04(14)
	808.1(5)	$11/2^+$	$7/2^+$	5.4(13)	21(4)		2.62(50)
978.2	397.2(2)	$9/2^-$	$7/2^-$	5.7(9)	11(2)	1.24(18)	
	538.8(8)	$9/2^-$	$5/2^-$	5.2(9)	10(2)		
	728.5(2)	$9/2^-$	$5/2^-$	33.9(9)	64(3)	1.14(15)	
	802.9(2)	$9/2^-$	$9/2^+$	4.3(12)	8(2)		
	816.3(2)	$9/2^-$	$7/2^+$	3.9(12)	7(2)		
1024.1	848.8(2)	$13/2^+$	$9/2^+$	100[e]	100	0.97(11)	
1126.6	951.3(2)	$11/2^+$	$9/2^+$	14(3)	58(9)	0.65(14)	
	964.7(2)	$11/2^+$	$7/2^+$	10(3)	42(9)	0.99(24)	
1172.2	364.2(4)	$9/2^-$	$7/2^-$	3.6(8)	18(3)	0.77(18)	1.14(12)
	733.1(3)	$9/2^-$	$5/2^-$	16.5(12)	82(3)	1.08(8)	1.58(12)
1282.5	474.8(5)	$(7/2^-)$	$7/2^-$	0.5(3)	29(17)		
	843.2(5)	$(7/2^-)$	$5/2^-$	1.2(7)	71(17)		
1351.2	179.3(3)	$11/2^-$	$9/2^-$	0.6(3)	2(1)	0.82(26)	
	373.0(3)	$11/2^-$	$9/2^-$	2.4(8)	7(2)	1.22(20)	
	543.4(3)	$11/2^-$	$7/2^-$	1.3(8)	4(2)	1.52(33)	
	770.5(2)	$11/2^-$	$7/2^-$	29.0(11)	87(3)	1.36(15)	
1616.3	443.9(3)	$11/2^-$	$9/2^-$	1.5(7)	18(8)	0.77(18)	
	808.4(4)	$11/2^-$	$7/2^-$	6.8(15)	82(8)	0.97(14)	1.57(12)
1620.8	824.3(7)	$(11/2^+)$	$7/2^+$	8.0(20)	100		
1721.9	595.3(3)	$13/2^+$	$11/2^+$	3.0(9)	15(4)		
	697.8(2)	$13/2^+$	$13/2^+$	2.3(9)	12(4)	0.78(18)	
	751.9(3)	$13/2^+$	$11/2^+$	14.3(13)	73(5)		1.17(14)
1886.3	535.3(5)	$13/2^-$	$11/2^-$	0.8(4)	3(1)		
	908.1(2)	$13/2^-$	$9/2^-$	25.2(12)	90(3)	1.08(13)	
	916.4(5)	$13/2^-$	$11/2^+$	2.0(8)	7(3)		
2055.4	1031.3(3)	$15/2^+$	$13/2^+$	6.5(16)	52(9)	0.28(6)	
	1085.4(3)	$15/2^+$	$11/2^+$	6.0(16)	48(9)	1.15(25)	
2091.8	475.2(4)	$13/2^-$	$11/2^-$	0.6(4)	4(3)		
	740.4(4)	$13/2^-$	$11/2^-$	1.3(7)	9(4)	0.92(16)	
	919.6(3)	$13/2^-$	$9/2^-$	13.1(8)	87(5)	1.10(10)	

TABLE I. (*Continued*).

E_{lev} (keV)	E_γ (keV)	I_i^π	I_f^π	I_γ [a]	BR (%)	R_{DCO} [b]	R_{DCO} [c]
2103.3	1079.2(2)	$17/2^+$	$13/2^+$	54.4(20)	100	1.01(6)[g]	2.29(30)[g]
2240.2	1113.6(2)	$15/2^+$	$11/2^+$	14.6(10)	82(6)	1.05(20)	
	1215.9(5)	$15/2^+$	$13/2^+$	3.2(12)	18(6)	0.38(10)	
2263.6	377.3(5)	$15/2^-$	$13/2^-$	0.8(6)	3(2)		
	912.4(3)	$15/2^-$	$11/2^-$	25.0(15)	97(2)	1.32(16)	
2580.1	959.3(7)	$(15/2^+)$	$(11/2^+)$	4.3(20)	100		
2610.8	994.5(2)	$15/2^-$	$11/2^-$	4.1(14)	100	1.08(18)	
2789.6	1067.7(2)	$17/2^+$	$13/2^+$	3.0(13)	100		2.93(50)
2818.0	1201.6(4)	$15/2^-$	$11/2^-$	2.2(11)	85(12)	1.14(28)	
	1466.8(8)	$15/2^-$	$11/2^-$	0.4(3)	15(12)		
2863.9	977.6(4)	$17/2^-$	$13/2^-$	19.6(20)	100	1.23(12)	
2868.9	777.1(5)	$(15/2^-)$	$13/2^-$	1.0(6)	67(19)		
	1253.6(5)	$(15/2^-)$	$11/2^-$	0.5(3)	33(19)		
2966.2	102.7(7)	$17/2^-$	$17/2^-$	0.8(4)	16(7)		
	355.5(4)	$17/2^-$	$15/2^-$	0.7(4)	14(7)		
	702.6(2)	$17/2^-$	$15/2^-$	1.1(4)	22(7)	0.58(14)	
	874.8(5)	$17/2^-$	$13/2^-$	2.4(7)	48(10)		
3014.4	922.2(5)	$17/2^-$	$13/2^-$	1.1(7)	10(6)		
	1128.1(5)	$17/2^-$	$13/2^-$	9.9(12)	90(6)	1.20(16)	
3071.7	808.0(8)	$17/2^-$	$15/2^-$	1.5(10)	25(13)		
	979.9(2)	$17/2^-$	$13/2^-$	3.7(7)	63(12)	1.24(22)	
	1185.6(5)	$17/2^-$	$13/2^-$	0.7(4)	12(7)		
3147.1	1055.3(3)	$17/2^-$	$13/2^-$	2.4(10)	100	0.92(15)	
3201.1	332.2(5)	$17/2^-$	$(15/2^-)$	1.4(8) [f]	58(20)	0.53(8)	
	383.1(5)	$17/2^-$	$15/2^-$	1.0(6)	42(20)	0.49(12)	
3245.5	1142.2(2)	$19/2^+$	$17/2^+$	4.2(6)	52(6)	0.36(6)	
	1190.1(2)	$19/2^+$	$15/2^+$	3.9(8)	48(6)		
3264.6	1001.0(3)	$19/2^-$	$15/2^-$	10.1(10)	100	0.99(8)	
3333.6	1230.3(2)	$21/2^+$	$17/2^+$	30.0(25)	100	1.07(8)	
3403.6	202.5(4)	$19/2^-$	$17/2^-$	0.6(3)	8(4)		
	389.2(2)	$19/2^-$	$17/2^-$	3.1(7)	40(7)	0.58(10)	
	437.0(6)	$19/2^-$	$17/2^-$	1.1(5)	14(6)		
	539.6(3)	$19/2^-$	$17/2^-$	2.2(5)	29(6)	0.60(14)	
	1140.0(5)	$19/2^-$	$15/2^-$	0.7(3)	9(4)		
3409.6	1169.4(3)	$19/2^+$	$15/2^+$	7.5(15)	100	1.00(20)	1.89(30)
3439.5	238.4(9)	$19/2^-$	$17/2^-$	1.5(10) [f]	21(12)		
	293(1)	$19/2^-$	$17/2^-$	0.8(4)	12(6)		
	425.3(8)	$19/2^-$	$17/2^-$	0.8(4)	12(6)		
	473.0(5)	$19/2^-$	$17/2^-$	1.1(6)	16(8)		
	575.0(2)	$19/2^-$	$17/2^-$	1.5(5)	22(7)	0.37(10)	
	1336.1(7)	$19/2^-$	$17/2^+$	1.2(7)	17(9)		
3471.5	399.6(6)	$19/2^-$	$17/2^-$	0.5(3)	12(7)		
	607.6(6)	$19/2^-$	$17/2^-$	1.4(5)	34(11)	0.47(12)	
	860.7(3)	$19/2^-$	$15/2^-$	1.1(6)	27(12)		
	1208.8(8)	$19/2^-$	$15/2^-$	1.1(6)	27(12)		
3641.8	1031(2)	$(19/2^-)$	$15/2^-$	0.3(2)	100		
3764.4	292.7(4)	$21/2^-$	$19/2^-$	2.1(15)[f]	16(10)		
	324.9(2)	$21/2^-$	$19/2^-$	2.7(9)	20(6)	0.53(18)	0.86(14)
	360.8(2)	$21/2^-$	$19/2^-$	2.8(9)	21(6)	0.49(10)	
	499.8(2)	$21/2^-$	$19/2^-$	0.8(4)	6(3)	0.40(12)	
	616.9(5)	$21/2^-$	$17/2^-$	0.8(4)	6(3)		
	693.1(3)	$21/2^-$	$17/2^-$	0.5(3)	4(2)		
	900.5(6)	$21/2^-$	$17/2^-$	3.6(10)	27(7)		
3864.5	530.9(2)	$21/2^+$	$21/2^+$	3.6(11)	80(10)	0.85(15)	1.72(35)
	619.0(4)	$21/2^+$	$19/2^+$	0.9(5)	20(10)		1.03(30)

TABLE I. (*Continued*).

E_{lev} (keV)	E_γ (keV)	I_i^π	I_f^π	I_γ[a]	BR (%)	R_{DCO}[b]	R_{DCO}[c]
3880.0	476.2(4)	$21/2^-$	$19/2^-$	0.7(4)	16(10)		
	1016.1(4)	$21/2^-$	$17/2^-$	3.8(18)	84(10)	1.09(25)	
3885.1	1095.5(4)	$(21/2^+)$	$17/2^+$	1.1(6)	46(17)		
	1781.7(4)	$(21/2^+)$	$17/2^+$	1.3(5)	54(17)		
3988.2	973.8(8)	$(21/2^-)$	$17/2^-$	0.5(3)	100		
4180.0	315.6(2)	$23/2^+$	$21/2^+$	1.1(6)	13(8)	0.49(9)	
	846.8(9)	$23/2^+$	$21/2^+$	6.0(30)[f]	72(12)	0.84(5)[g]	
	934.8(3)	$23/2^+$	$19/2^+$	1.3(6)	15(8)		
4301.1	536.7(2)	$23/2^-$	$21/2^-$	2.3(5)	53(8)	0.68(14)	
	1037.0(2)	$23/2^-$	$19/2^-$	2.0(5)	47(8)	1.10(24)	
4320.7	556.3(3)	$23/2^-$	$21/2^-$	1.9(5)	59(11)		
	1056.1(3)	$23/2^-$	$19/2^-$	1.3(5)	41(11)	1.21(24)	
4391.6	1127(2)	$(23/2^-)$	$19/2^-$	2.5(10)	100		
4531.7	1198.1(3)	$(23/2^+)$	$21/2^+$	0.8(4)	73(17)		
	1286.3(4)	$(23/2^+)$	$19/2^+$	0.3(2)	27(17)		
4625.7	445.3(7)	$25/2^+$	$23/2^+$	0.6(4)	8(6)		
	1292.1(3)	$25/2^+$	$21/2^+$	6.8(30)	92(6)	0.93(14)	
4670.5	1260.9(6)	$(23/2^+)$	$19/2^+$	1.1(5)	100		
4846.6	525.9(3)	$(25/2^-)$	$23/2^-$	1.2(5)	60(16)		
	1082.1(9)	$(25/2^-)$	$21/2^-$	0.8(4)	40(16)		
4862.1	236.4(3)	$25/2^+$	$25/2^+$	1.2(6)	18(8)	1.51(45)	
	682.0(3)	$25/2^+$	$23/2^+$	4.1(8)[f]	60(9)	0.55(10)[g]	
	997.8(7)	$25/2^+$	$21/2^+$	0.5(3)	7(4)		
	1528.5(4)	$25/2^+$	$21/2^+$	1.0(6)	15(8)		
5001.0	1121(2)	$(25/2^-)$	$21/2^-$	1.6(7)	100		
5258.7	633.0(3)	$27/2^+$	$25/2^+$	3.2(8)	76(12)	0.48(8)	
	1078.8(7)	$27/2^+$	$23/2^+$	1.0(6)[f]	24(12)	1.01(6)[g]	2.29(30)[g]
5583	1192(2)	$(27/2^-)$	$(23/2^-)$	0.4(6)	100		
5942	682(2)	$(29/2^+)$	$27/2^+$	1.0(7)[f]	32(18)	0.55(10)[g]	
	1316(2)	$(29/2^+)$	$25/2^+$	2.1(9)	68(18)		
6655	1396(2)	$(31/2^+)$	$27/2^+$	2.1(10)	100		

[a]Intensities determined from triangular array.
[b]DCO ratio determined from $E2$ gate.
[c]DCO ratio determined from $\Delta I=1$ gate.
[d]Not observed. Taken from Ref. [14].
[e]Normalization.
[f]Intensity estimate due to strong doublet.
[g]DCO ratio of the doublet.

ment of the 682 keV doublet is also supported by gate-dependent intensity variations.

Spin assignments to the new levels are based on the DCO ratios determined from gates on both $\Delta I=1$ and $\Delta I=2$ transitions. The DCO ratio of the 849 keV line in the 1292 keV gate, which excludes the 847 keV line, is close to unity. In other gates, the DCO ratio of the 847-849 keV doublet varied below unity in a pattern consistent with about 0.5 for the 847 keV decay and unity for the 849 keV line. The DCO ratios for the 1079 keV doublet were close to unity in all $\Delta I=2$ gates, consistent with a value of 1.0 for both transitions. Separate DCO ratios could not be determined for the two 682 keV transitions. Since the $\frac{25}{2}^+ \rightarrow \frac{23}{2}^+$ decay is considerably stronger than the $(\frac{29}{2}^+) \rightarrow \frac{27}{2}^+$ decay, the measured DCO ratio of 0.55(10) is believed to represent mainly that of the former transition.

B. Other positive-parity bands

A second positive-parity structure was known up to the 2790 keV level [13], although no spin assignments above the $(\frac{13}{2}^+)$ 1722 keV level were given. The two signature partners were extended up to the $(\frac{23}{2}^+)$ 4671 keV and the $(\frac{21}{2}^+)$ 3885 keV levels. Spin assignments were made up to the $\frac{19}{2}^+$ 3410 keV level based on several DCO values as shown in Table I. Tentative assignments were made for the top two states based on systematics.

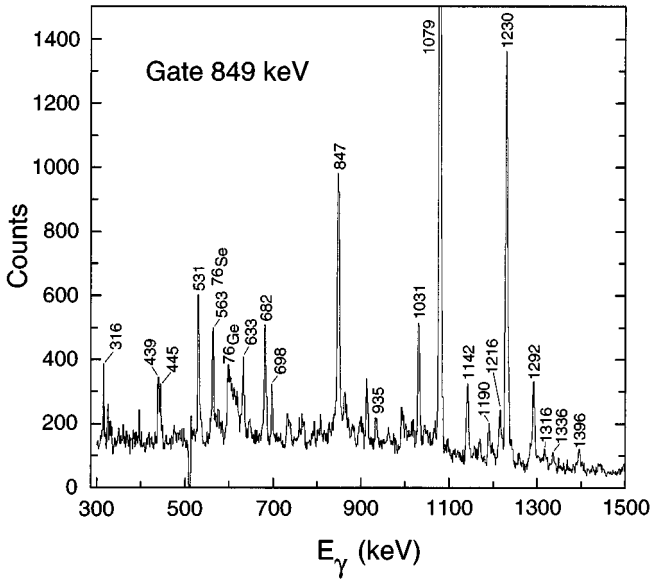

FIG. 2. Portion of a background-corrected spectrum in coincidence with the 849 keV transition in the yrast positive-parity band.

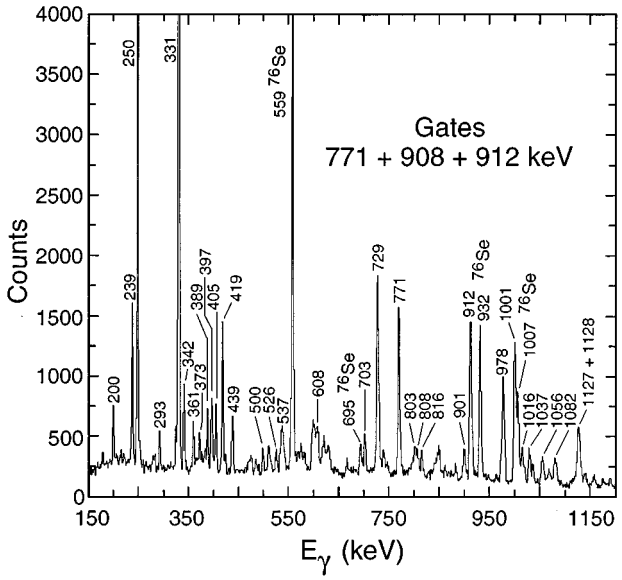

FIG. 3. Portion of a background-corrected sum coincidence spectrum gated on the 771, 908, and 912 keV transitions in the lowest negative-parity band.

Another positive-parity structure was known [14] up to the $\frac{7}{2}^+$ 797 keV level. This has been confirmed in the present work and extended up to the $(\frac{15}{2}^+)$ 2580 keV level by the addition of two new transitions. Tentative spin assignments were made based on systematics.

C. Lowest negative-parity band

The $\alpha=+\frac{1}{2}$ signature of the yrast negative-parity band was previously known [12] up to the $(\frac{13}{2}^-)$ 1886 keV level. Honusek *et al.* [13] extended this signature up to the 3880 keV $(\frac{21}{2}^-)$ level. The signature partner band was known [13] up to the $(\frac{19}{2}^-)$ 3265 keV level. The present work has confirmed these results and extended the $\alpha=+\frac{1}{2}$ signature band up to the 5001 keV $(\frac{25}{2}^-)$ level and the $\alpha=-\frac{1}{2}$ band up to the 5583 keV $(\frac{27}{2}^-)$ level. A sum of coincidence spectra in this band is shown in Fig. 3 to illustrate the data. Spin as-

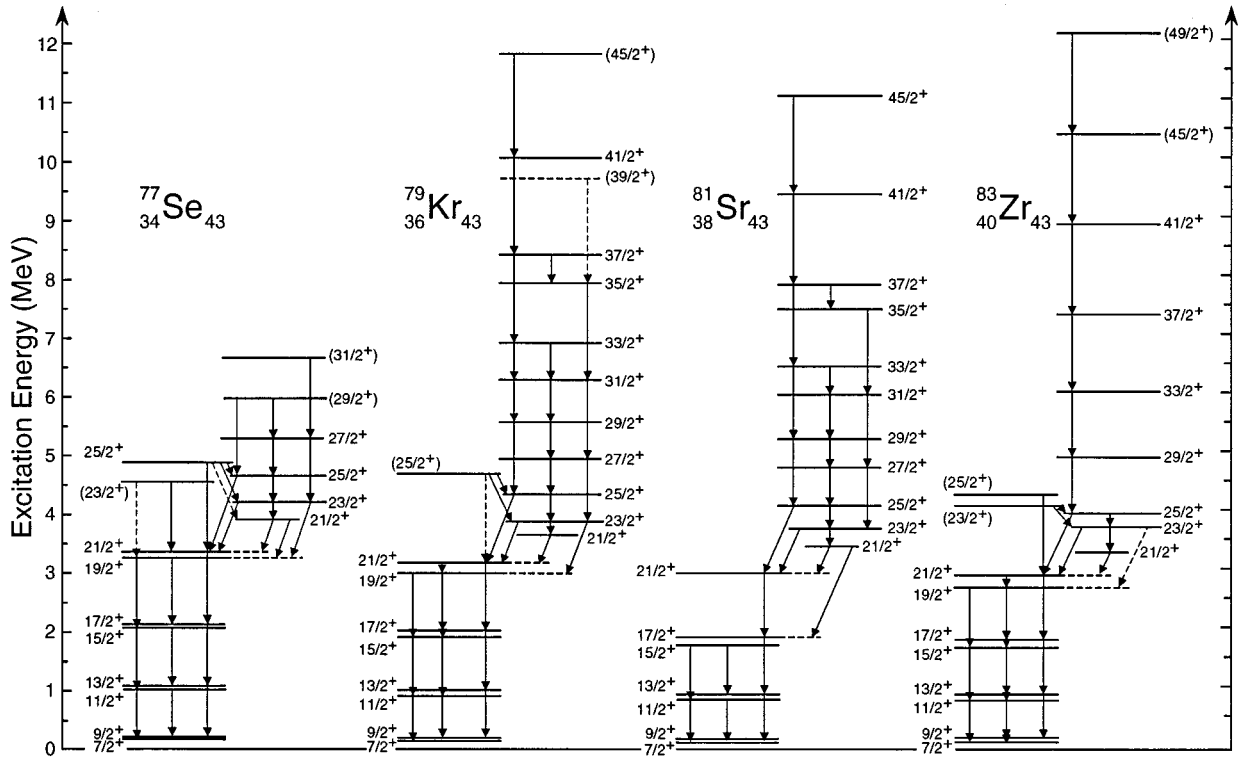

FIG. 4. Comparison of the yrast positive-parity bands in ^{77}Se, ^{79}Kr [5–7], ^{81}Sr [1–4], and ^{83}Zr [8–11]. The $\frac{19}{2}^+$ state is not known in ^{81}Sr.

signments of the $\frac{11}{2}^-$ through $\frac{21}{2}^-$ levels were made based on DCO values close to unity for deexciting $\Delta I=2$ transitions.

The $\Delta I=1$ sequence was extended up to the $\frac{15}{2}^-$ 2264 keV level. The large DCO ratios for these $\Delta I=1$ decays are consistent with previously measured angular distributions [12,16] and imply large $E2/M1$ mixing ratios of 0.5–1.0. These mixing and branching ratios and the measured lifetimes of 49(9) and 1.0(4) ps [16] for the levels at 581 and 978 keV, respectively, show that the $M1$ strengths are very weak in this band [$B(M1) \sim 0.01$ Weisskopf units (W.u.)], while the $E2$ strengths are considerably enhanced [$B(E2) \sim 100$ W.u.]. Two new transitions at 803 and 916 keV which decay to the positive-parity yrast structure were also found. In addition, three new transitions were placed which decay to the $\frac{1}{2}^-$ band.

D. Other negative-parity bands

The ground-state band was previously known [13] up to the 2611 keV $\frac{15}{2}^-$ level. The present work confirmed these results and extended the structure up to a tentative 3642 keV ($\frac{19}{2}^-$) level. DCO values close to unity for $\Delta I=2$ transitions were used to make spin assignments for the $\frac{11}{2}^-$ through $\frac{17}{2}^-$ states. The $\Delta I=1$ branching and DCO ratios indicate that the $M1$ strengths are more normal in this band, that is, an order of magnitude or more higher than in the $\frac{5}{2}^-$ band.

Some candidates for a high-lying high-K negative-parity structure were identified [13] previously at excitation energies of 3014 and 3404 keV. No spin assignments were given. This work has confirmed these states and added 11 new ones with numerous deexciting transitions to both negative-parity structures and to the positive-parity yrast band. Many of these lines can be seen in Fig. 3.

A low-lying structure consisting of the 520 and 824 keV levels was reported in Ref. [14]. These levels were confirmed in the present work and one additional ($\frac{7}{2}^-$) level at 1283 keV has been added.

IV. DISCUSSION

A. Positive-parity bands

One of the most striking features of the level scheme of ^{77}Se is the abrupt change of signature splitting in the yrast positive-parity band at the $\frac{21}{2}^+$ levels. As shown in Fig. 4, a similar change has been seen in the heavier $N=43$ isotones ^{79}Kr [5–7], ^{81}Sr [1–4], and ^{83}Zr [8–11]. This behavior appears to be a characteristic of the $N=43$ isotones. As will be discussed below, it seems to result from a shape change caused by a $g_{9/2}$ quasiproton alignment. It is interesting that the 1qp band can be observed somewhat past the point at which it ceases to be yrast.

A cranked-shell-model analysis is quite useful in studying the rotational properties of these bands. As was done for ^{79}Kr [6], the lower $\frac{21}{2}^+$ state was used since it is connected to the other members of the band by electric quadrupole transitions, whereas the upper $\frac{21}{2}^+$ state is not. This allows the entire positive-parity sequence to be treated as a continuous structure. An effective K value of $\frac{5}{2}$ was employed to facilitate comparisons with the other $N=43$ isotones.

A comparison of the kinematic moments of inertia $J^{(1)}$ versus rotational frequency for the yrast positive-parity band in ^{77}Se, ^{79}Kr [5–7], ^{81}Sr [1–4], and ^{83}Zr [8–11] is shown in Fig. 5. In general, an overall similarity can be seen. The favored $\alpha=+\frac{1}{2}$ signature shows a sharp upbend at a rotational frequency of about $\hbar\omega \approx 0.55$ MeV. This upbend has been interpreted as the alignment of a pair of $g_{9/2}$ quasiprotons at the $\frac{21}{2}^+$ level, leading to the 3qp configuration $\nu g_{9/2} \otimes \pi g_{9/2}^2$. This band crossing appears to become sharper with increasing mass. The $\alpha=-\frac{1}{2}$ signature shows a sharp backbend at about the same rotational frequency.

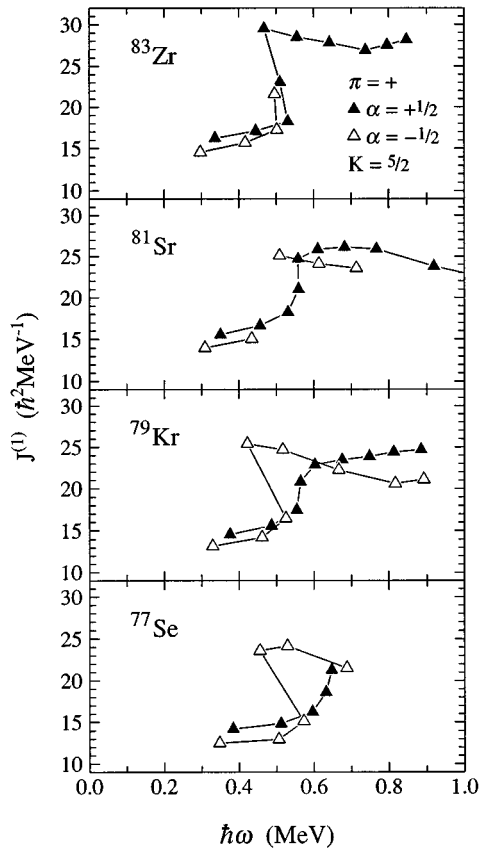

FIG. 5. Kinematic moments of inertia $J^{(1)}$ versus rotational frequency $\hbar\omega$ for the positive-parity yrast bands in ^{83}Zr [8–11], ^{81}Sr [1–4], ^{79}Kr [5–7], and ^{77}Se. The $\alpha=-\frac{1}{2}$ curve for ^{81}Sr is broken because the $\frac{19}{2}^+$ state has not been experimentally located.

The experimental Routhian curves are plotted versus rotational frequency for the isotones in Fig. 6. To allow comparisons with other $N=43$ nuclei, the same reference rotor parameters were used in this analysis as were used in other analyses [1,5,6], $J_0=11\hbar^2/\text{MeV}$ and $J_1=0\hbar^3/\text{MeV}^4$. A qualitatively similar signature splitting pattern can be seen. Large signature splitting is prevalent before the first crossing, but after the $g_{9/2}$ quasiproton alignment, the signature splitting vanishes. For the nuclei which are known to higher spins, a return of large signature splitting is also seen at higher frequencies.

The deformed Woods-Saxon cranking model [20] was used to calculate shape and deformation in ^{77}Se. A monopole pairing force was used in the cranking calculations. The Routhians were calculated for a range of shape parameters β_2 and γ and minimized with respect to the hexadecapole deformation β_4. Figure 7 shows three total Routhian surface

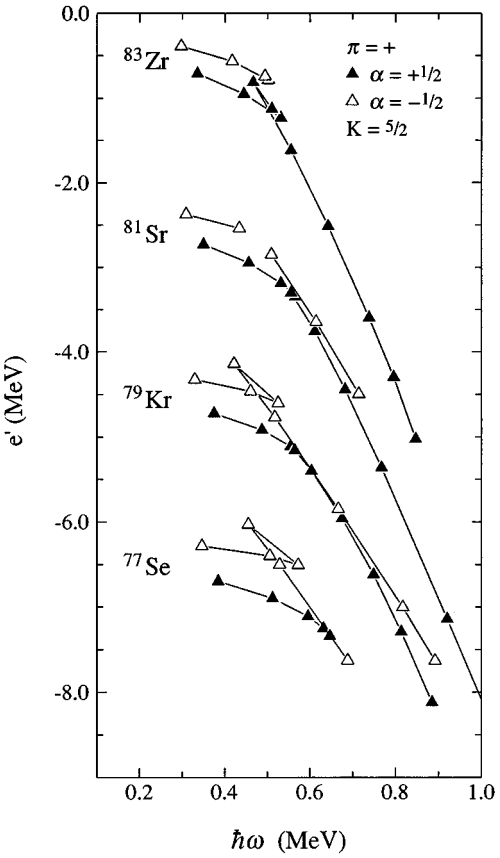

FIG. 6. Experimental Routhians e' as a function of rotational frequency $\hbar\omega$ for the yrast positive-parity states in ^{83}Zr [8–11], ^{81}Sr [1–4], ^{79}Kr [5–7], and ^{77}Se. Harris parameters $J_0 = 11\hbar^2$/MeV and $J_1 = 0\hbar^3$/MeV^4 were used for the reference rotor. The Routhians for ^{81}Sr, ^{79}Kr, and ^{77}Se have been shifted down by -2, -4, and -6 MeV, respectively.

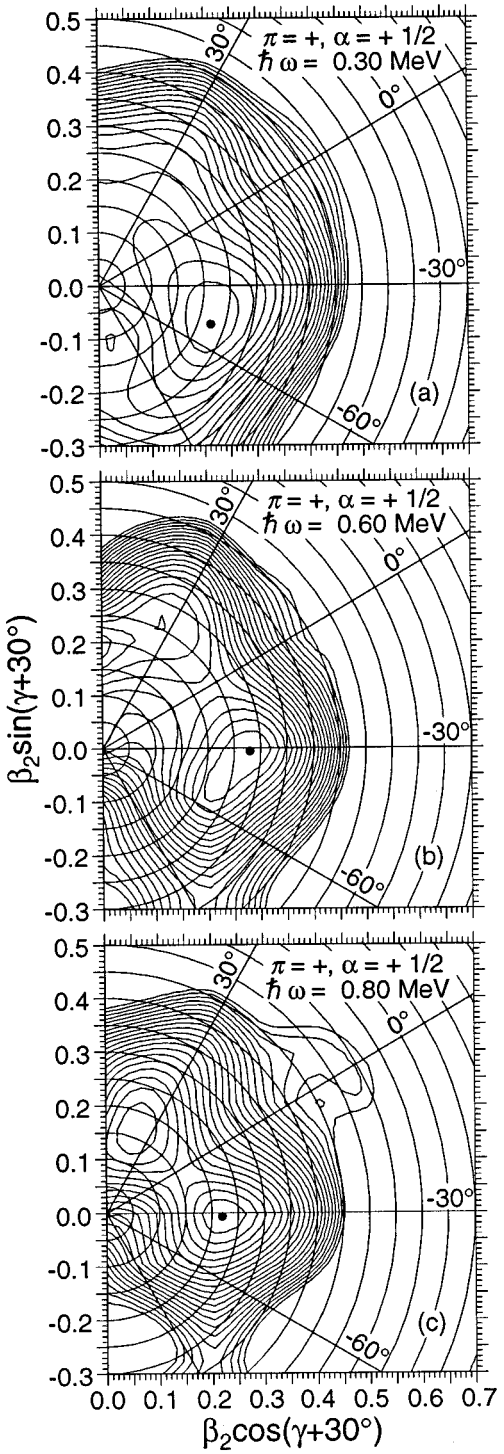

FIG. 7. Total Routhian surfaces in the (β_2,γ) polar coordinate plane for the $\alpha = +\frac{1}{2}$ signature positive-parity states in ^{77}Se. The separation between contour lines is 200 keV. In these graphs collective rotation for prolate and oblate shapes occurs at $\gamma = 0°$ and $-60°$, respectively.

(TRS) plots for the favored signature of the positive-parity yrast band in ^{77}Se.

For a rotational frequency of $\omega = 0.30$ MeV/$\hbar$, which lies below the first band crossing, a near-oblate shape ($\gamma \approx -50°$) is predicted with a deformation of about $\beta_2 \approx 0.22$. This shape gives rise to the large signature splitting seen experimentally, as it also does in the heavier $N = 43$ isotones.

After the first crossing, at a rotational frequency of $\omega = 0.60$ MeV/$\hbar$, the deformation has increased somewhat to $\beta_2 \approx 0.28$. The shape has also shifted to a triaxial shape with $\gamma \approx -30°$, leading to reduced signature splitting. At an even higher rotational frequency, $\omega = 0.80$ MeV/$\hbar$, the shape is predicted to remain triaxial with a somewhat lower deformation of $\beta_2 \approx 0.22$, unlike the case in ^{79}Kr where a return to an oblate shape is predicted to lead to increased signature splitting. This theoretical prediction for ^{77}Se differs substantially from that for the heavier $N = 43$ isotones. An experimental test would be very interesting, but it is difficult to produce ^{77}Se with sufficient angular momentum, due to its inaccessibility to heavy-ion reactions.

Two additional positive-parity bands with bandhead spins of $\frac{5}{2}^+$ and $\frac{11}{2}^+$ at 302 and 1127 keV, respectively, were seen in ^{77}Se. Analogs of both of these bands were seen in ^{79}Kr [5], and the $(\frac{5}{2}^+)$ and $(\frac{7}{2}^+)$ levels reported at 203 and 612 keV in ^{81}Sr [4] may represent the beginning of a band analogous to the $\frac{5}{2}^+$ band in ^{77}Se. A configuration of $\nu[422]\frac{5}{2}$ has been assigned to this bandhead [1] in ^{81}Sr.

A particle-plus-triaxial-rotor model calculation was performed to see how well the three 1qp positive-parity bands could be reproduced with a single shape. The codes GAMPN,

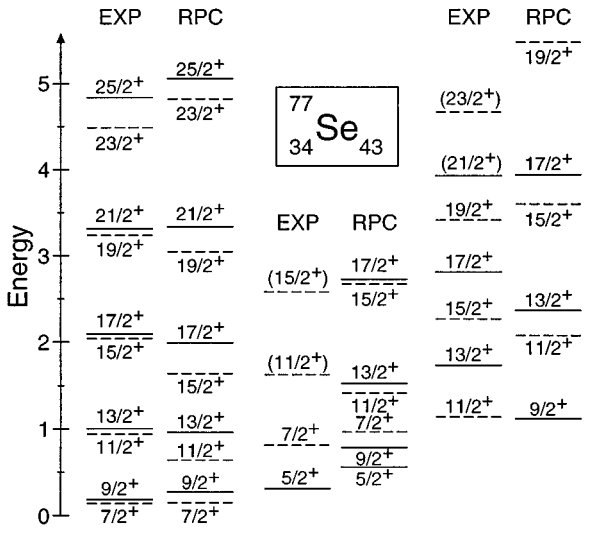

FIG. 8. A comparison of levels predicted by rotation-particle coupling calculations with observed positive-parity levels. The shape and moment of inertia parameters were $\epsilon_2=-0.20$, $\gamma=11.3°$, $\epsilon_4=0.027$, and $E_{2^+}=320$ keV.

ASYRMO, and PROBAMO [21,22] were used with standard parameters [23] for the modified harmonic oscillator potential. The shape parameters used ($\epsilon_2=-0.20$, $\gamma=11.3°$, and $\epsilon_4=0.027$) correspond to the Woods-Saxon shape parameters at the minimum in the TRS calculations for $\hbar\omega=0.30$ MeV. Since the predicted shape is nearly oblate, the calculation was based on a small degree of triaxiality away from an oblate shape, rather than a large deviation from a prolate shape. A constant moment of inertia corresponding to a 2^+ energy of 320 keV was used for the rotating core. Although this is smaller than the observed value of 559 keV in ^{76}Se, the 2^+ energy in the light even-even Se isotopes is known to be significantly larger than what would be implied by the spacing of the higher-spin states due to shape coexistence [24,25].

Calculations were made previously [21] for ^{77}Se using the same rotation-particle-coupling (RPC) codes. These calculations, performed before theoretical shape predictions were available, used the shape parameters $\epsilon_2=0.29$, $\gamma=30°$, and $\epsilon_4=0$ and a moment of inertia corresponding to a 2^+ energy in the core of 600 keV for both the positive- and negative-parity bands. A comparison between these calculations and the present ones indicates the degree of parameter dependence.

The energy levels predicted by the rotation-particle-coupling model are compared with the observed ones in Fig. 8. The theoretical states connected by large $B(E2)$ strengths were grouped into bands. The $\frac{7}{2}^+$ bandhead is correctly predicted below the $\frac{5}{2}^+$ bandhead. The energies of the states in the $\frac{7}{2}^+$ band are reproduced reasonably well, although the degree of signature splitting is somewhat underpredicted. The earlier RPC calculations [21] also give a reasonable reproduction of the band, but overpredict the degree of signature splitting. Thus the agreement in signature splitting could probably be improved by varying the triaxiality parameter γ, but no attempt was made to vary the RPC parameters to fit the data.

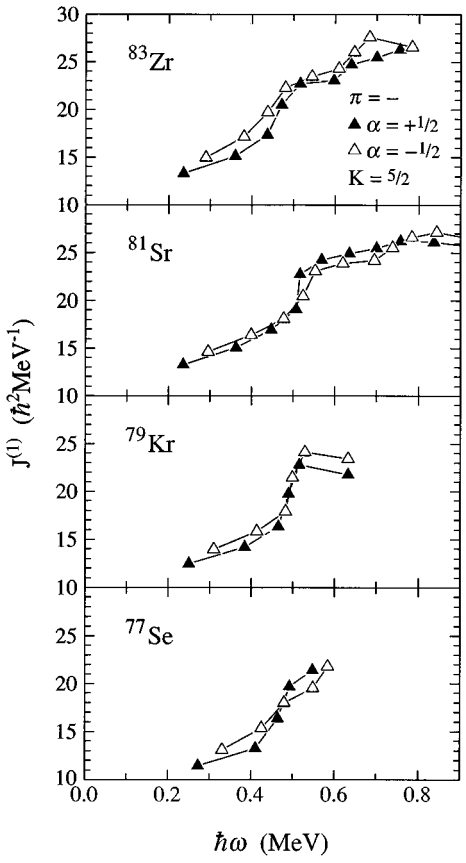

FIG. 9. Kinematic moments of inertia $J^{(1)}$ versus rotational frequency $\hbar\omega$ for the lowest negative-parity yrast bands in ^{83}Zr [8–11], ^{81}Sr [1–4], ^{79}Kr [5–7], and ^{77}Se.

At this shape the next predicted band is based on a $\frac{5}{2}^+$ state. For comparison, the experimentally observed decay sequence ending on the 302 keV $\frac{5}{2}^+$ level is shown, although it is by no means clear that the experimental and theoretical structures correspond. A correspondence would be more likely if the 797 keV state had spin $\frac{9}{2}$ rather than $\frac{7}{2}$, since the predicted large signature splitting would strongly favor population of the $\alpha=+\frac{1}{2}$ band. However, the spin assignment of $\frac{7}{2}$ for the 302 keV state appears rather strong because it is based on both the DCO ratio observed here for the decay line and on the population of this state in the neutron capture experiment [14] which strongly favored low-spin states.

The third band predicted theoretically is built on a $\frac{9}{2}^+$ bandhead. This is compared with the third experimentally observed band in Fig. 8, but the agreement is not very good. The predicted band lies too high, shows too much signature splitting, and starts with a $\frac{9}{2}^+$ state for which no experimental counterpart is known. This may indicate that the $\frac{11}{2}^+$ band is based on a completely different shape.

B. Negative-parity bands

Three negative-parity bandheads lie at relatively low excitation energies. The $\frac{1}{2}^-$ bandhead forms the ground state of ^{77}Se, while the $\frac{5}{2}^-$ band is yrast and most strongly populated among the negative-parity states, and the $\frac{3}{2}^-$ state lies highest and is the most weakly populated. Exactly the same situation occurs in the $N=43$ isotones ^{79}Kr [5], ^{81}Sr [4], and

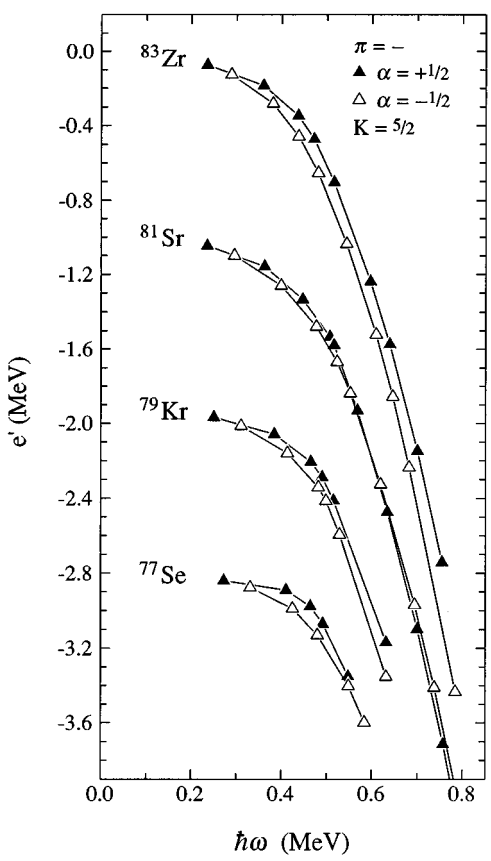

FIG. 10. Experimental Routhians e' as a function of rotational frequency $\hbar\omega$ for the lowest negative-parity states in ^{83}Zr [8–11], ^{81}Sr [1–4], ^{79}Kr [5–7], and ^{77}Se. Harris parameters $J_0=11\hbar^2/\mathrm{MeV}$ and $J_1=0\hbar^3/\mathrm{MeV}^4$ were used for the reference rotor. The Routhians for ^{81}Sr, ^{79}Kr, and ^{77}Se have been shifted down by -1, -2, and -3 MeV, respectively.

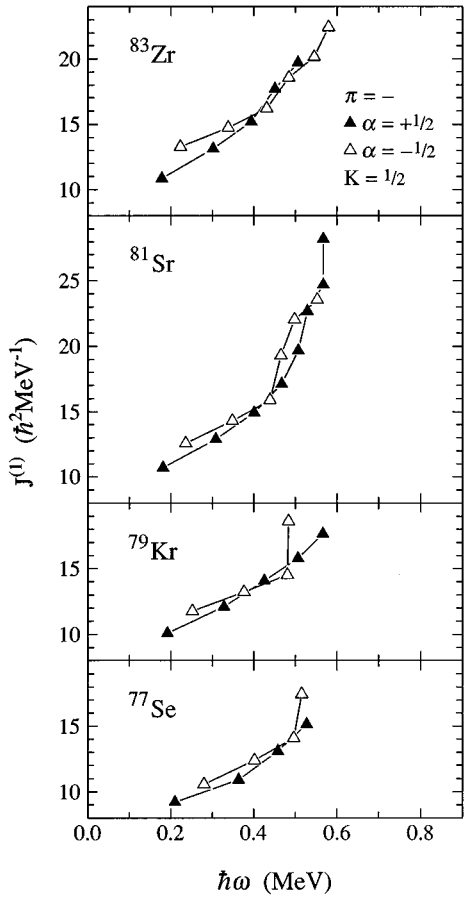

FIG. 11. Kinematic moments of inertia $J^{(1)}$ versus rotational frequency $\hbar\omega$ for the negative-parity ground state bands in ^{83}Zr [8–11], ^{81}Sr [1–4], ^{79}Kr [5–7], and ^{77}Se.

^{83}Zr [9,11]. These three bandheads have been interpreted [1] to represent the configurations $\nu[301]\frac{1}{2}$, $\nu[303]\frac{5}{2}$, and $\nu[301]\frac{3}{2}$, respectively, all of which are predicted to lie relatively low in energy at a moderately deformed prolate shape ($\beta_2=0.3$).

As mentioned earlier, the $M1$ strengths are abnormally low in the $\frac{5}{2}^-$ band, but relatively normal in the $\frac{1}{2}^-$ ground-state band. This is also true in ^{79}Kr, where the difference has been attributed [7] to the single-particle configurations. The neutron gyromagnetic ratios were calculated to be $g_{K=1/2}=2.44$ and $g_{K=5/2}=0.49$ for pure Nilsson $\nu[301]\frac{1}{2}$ and $\nu[303]\frac{5}{2}$ states, respectively. Since the gyromagnetic ratio for collective rotation, $g_R\approx Z/A=0.46$, and $M1$ strengths are proportional to the difference g_K-g_R, a near cancellation occurs in the $\frac{5}{2}^-$ band, but not for the $\frac{1}{2}^-$ structure. This result is also confirmed by the RPC calculations discussed below.

It is instructive to compare the rotational properties of these negative-parity bands in ^{77}Se with the analogous structures in the heavier $N=43$ isotones. The kinematic moments of inertia $J^{(1)}$ and quasiparticle Routhian curves determined from a cranked-shell-model analysis for the $\frac{5}{2}^-$ bands are shown in Figs. 9 and 10, respectively. An effective K value of $\frac{5}{2}$ and a common set of Harris parameters of $J_0=11\hbar^2/\mathrm{MeV}$ and $J_1=0\hbar^3/\mathrm{MeV}^4$ for the reference rotor were used for the nuclei. A strong family resemblance can be seen.

An upbend in $J^{(1)}$ around $\hbar\omega\approx0.5$ MeV in all the nuclei shown in Fig. 9 indicates a quasiparticle alignment. A $g_{9/2}$ quasiproton alignment was suggested for ^{79}Kr [5] based on the similar crossing frequency observed in the yrast band. There is some evidence for the beginning of a second crossing at $\hbar\omega\approx0.6$ MeV in the $\alpha=-\frac{1}{2}$ signatures of ^{77}Se and ^{83}Zr. Since there is no Pauli blocking of the first neutron or proton alignments in these negative-parity bands, the neutron and proton alignments can be close in frequency.

The Routhians in Fig. 10 show that the signature splitting is much smaller than in the yrast positive-parity band and has the opposite sign; i.e., the $\alpha=-\frac{1}{2}$ signature is energetically favored. The splitting starts at nearly 0, increases to about 50–100 keV, and then decreases again at the first alignment, except for ^{83}Zr.

The kinematic moments of inertia in the somewhat less explored $\frac{1}{2}^-$ bands are compared in Fig. 11. Evidence can be seen in all four isotones for an alignment, or the beginnings of one, around or below a rotational frequency of 0.5 MeV/$\hbar$. In most cases, the rise appears to be sharper in the $\alpha=-\frac{1}{2}$ signature.

An interesting pattern can be seen in the Routhians for this band, shown in Fig. 12. In ^{83}Zr, the $\alpha=-\frac{1}{2}$ signature is energetically favored, as in the $\frac{5}{2}^-$ band, and the separation is also in the range of 50–100 keV. With decreasing Z, the

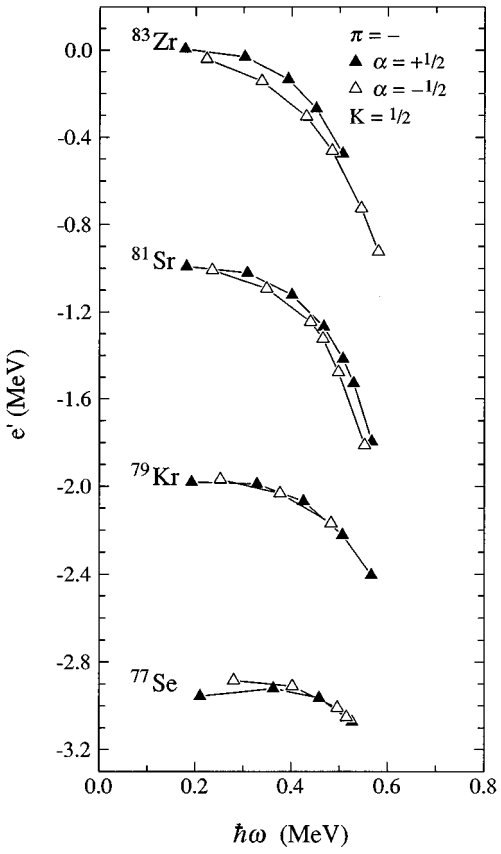

FIG. 12. Experimental Routhians e' as a function of rotational frequency $\hbar\omega$ for the ground state negative-parity bands in ^{83}Zr [8–11], ^{81}Sr [1–4], ^{79}Kr [5–7], and ^{77}Se. Harris parameters $J_0 = 11\hbar^2/\text{MeV}$ and $J_1 = 0\hbar^3/\text{MeV}^4$ were used for the reference rotor. The Routhians for ^{81}Sr, ^{79}Kr, and ^{77}Se have been shifted down by -1, -2, and -3 MeV, respectively.

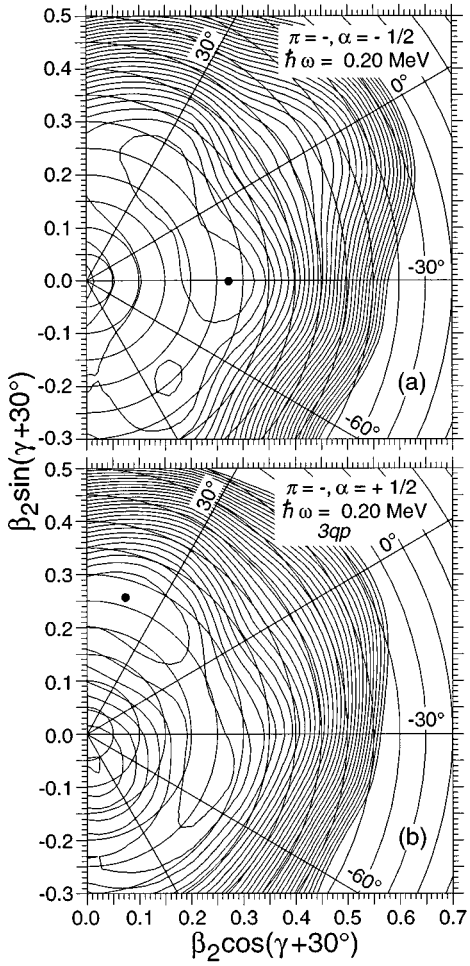

FIG. 13. Total Routhian surfaces in the (β_2, γ) polar coordinate plane for the (a) lowest negative-parity configuration and (b) other negative-parity states in ^{77}Se. The distance between contour lines in 250 keV.

energy of the $\alpha = -\frac{1}{2}$ signature increases relative to that of the $\alpha = +\frac{1}{2}$ signature. This leads to lower signature splitting in ^{81}Sr, almost none in ^{79}Kr, and reversed splitting, with the $\alpha = +\frac{1}{2}$ signature favored, in ^{77}Se.

A TRS graph typical for the 1qp negative-parity structures is shown in Fig. 13(a). The graph shows considerable γ softness with minima at three quite different γ values. The minimum at $(\beta_2, \gamma) = (0.26, 22°)$ is close to the shape identified for the $\frac{5}{2}^-$ band in ^{79}Kr [5]. This positive γ value reproduces the experimental observation that the $\alpha = -\frac{1}{2}$ signature is energetically favored in the $\frac{5}{2}^-$ band. The $(\beta_2, \gamma) = (0.27, -30°)$ minimum may be identified with the $\frac{1}{2}^-$ band. This shape would imply an energetically favored $\alpha = +\frac{1}{2}$ signature in agreement with experiment. The variation of signature splitting in the $\frac{1}{2}^-$ band could be accounted for by a decrease in the γ deformation parameter from positive to negative values with decreasing Z (see Fig. 13 of Ref. [5]).

An RPC calculation was also performed for a shape corresponding to that predicted by the TRS, i.e., $\epsilon_2 = 0.26$, $\gamma = 23.2°$, and $\epsilon_4 = 0.023$. The moment of inertia ($E_{2^+} = 320$ keV) was the same as that used for the positive-parity calculations. No parameters were varied to improve agreement with experiment. The calculated states were grouped into bands based on the predicted $E2$ decay strengths and are compared with the observed bands in Fig. 14.

The negative-parity structures are reproduced reasonably well. The $\frac{1}{2}^-$ bandhead is predicted somewhat above the $\frac{5}{2}^-$ bandhead, but the opposite is true experimentally. However, this is only a question of a few hundred keV and may be sensitive to the triaxiality parameter γ. In fact the earlier RPC calculations [21] with different shape parameters do predict the correct ordering of the bandheads. The degree of signature splitting is predicted well for the $\frac{5}{2}^-$ band, but not for the $\frac{1}{2}^-$ or $\frac{3}{2}^-$ bands. In comparison, the earlier calculations predict the degree of signature splitting better in the $\frac{1}{2}^-$ band than in the $\frac{5}{2}^-$ band.

The $E2/M1$ mixing ratios δ from the RPC calculations for the $\Delta I = 1$ transitions in the $\frac{1}{2}^-$ and $\frac{5}{2}^-$ bands are listed in Table II. These values of δ are based on the theoretically predicted $B(E2)$ and $B(M1)$ strengths and on the experimentally observed γ-ray energies. Most of those in the $\frac{1}{2}^-$ band are relatively low ($0.1 \leqslant \delta \leqslant 0.3$) and would imply DCO ratios around $\frac{1}{2}$, in general agreement with experiment. On the other hand, large, mostly negative, mixing ratios are predicted for the $\Delta I = 1$ transitions in the $\frac{5}{2}^-$ band. These are qualitatively consistent with the large DCO ratios observed in this band. The predicted $B(E2)$ strengths are similar in the

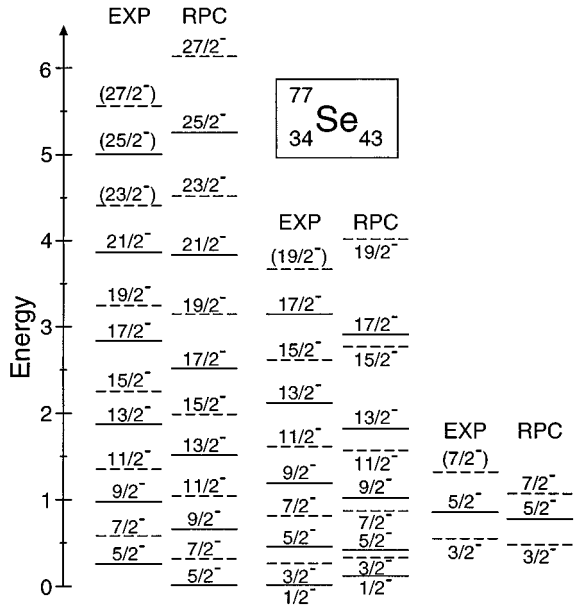

FIG. 14. A comparison of levels predicted by rotation-particle coupling calculations with observed negative-parity levels. The shape and moment of inertia parameters were $\epsilon_2=0.26$, $\gamma=23.2°$, $\epsilon_4=0.023$, and $E_{2^+}=320$ keV.

two bands. The differences in the DCO ratios arise mainly from the predicted differences in the $B(M1)$ strengths, which are much weaker in the $\frac{5}{2}^-$ band due to the near cancellation between the single-particle and rotational magnetic moments. The cancellation is extremely close for the 331 keV transition, leading to the large positive predicted mixing ratio. Slight changes in the calculation might reduce the cancellation and give a value of δ more like that of the higher transitions.

C. High-lying high-K structure

A complex of high-lying negative-parity states starting at 2818 keV can be seen in Fig 1. Most are likely to represent 3qp configurations since the first crossings occur in the other bands at about this excitation energy. $\Delta I=1$ transitions are much more common than $\Delta I=2$ decays among these states. Similar states have been seen in the isotone ^{79}Kr [5] and in a number of odd-Z nuclei [17], but never in such large numbers.

TABLE II. $B(E2)/B(M1)$ mixing ratios δ from particle-rotor model calculations.

Band	E_γ (keV)	$I_i^\pi \rightarrow I_f^\pi$	δ
$\frac{1}{2}^-$	239	$\frac{3}{2}^- \rightarrow \frac{1}{2}^-$	0.26
	200	$\frac{5}{2}^- \rightarrow \frac{3}{2}^-$	0.23
	369	$\frac{7}{2}^- \rightarrow \frac{5}{2}^-$	0.10
	364	$\frac{9}{2}^- \rightarrow \frac{7}{2}^-$	0.27
	444	$\frac{11}{2}^- \rightarrow \frac{9}{2}^-$	0.55
$\frac{5}{2}^-$	331	$\frac{7}{2}^- \rightarrow \frac{5}{2}^-$	72
	397	$\frac{9}{2}^- \rightarrow \frac{7}{2}^-$	−6.9
	373	$\frac{11}{2}^- \rightarrow \frac{9}{2}^-$	−3.6
	535	$\frac{13}{2}^- \rightarrow \frac{11}{2}^-$	−2.6
	377	$\frac{15}{2}^- \rightarrow \frac{13}{2}^-$	−1.5

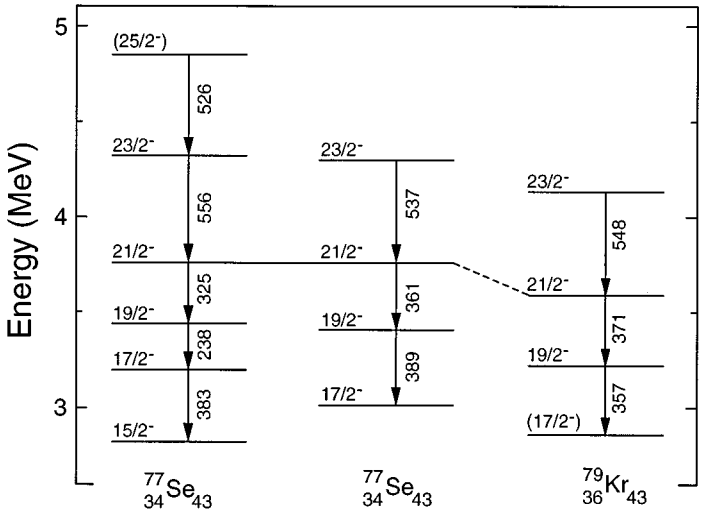

FIG. 15. Comparison of negative-parity 3qp band structures in ^{77}Se and ^{79}Kr [5,6].

Some $\Delta I=1$ decay sequences from this complex have been selected for comparison with the possibly analogous structure in ^{79}Kr and are shown in Fig. 15. The sequence shown in the middle resembles that in ^{79}Kr the best, but the left sequence shows that there are other candidates. Note also that the same $\frac{21}{2}^-$ level is shared in the two ^{77}Se decay sequences and the sequences above or below this level could be exchanged.

Three-quasiparticle configurations of the generic form $\pi[fp]\otimes\pi g_{9/2}\otimes\nu g_{9/2}$ (for an odd-N nucleus) have been proposed for such sequences in other nuclei. The predicted shape for such a configuration, shown in Fig. 13(b), is $(\beta_2,\gamma)=(0.27,44°)$, which is close to the noncollective $\gamma=60°$ axis. The $\frac{17}{2}^-$ structure in ^{79}Kr has been associated [5] with a noncollective oblate shape with the configuration $\pi[(g_{9/2})_{9/2^+}\otimes(p_{3/2}\oplus f_{5/2})_{3/2^-}]_{6^-}\otimes\nu(g_{9/2})_{5/2^+}$ as the bandhead. This differs from the 3qp configurations formed after a pair alignment in the lower negative- or positive-parity bands, which are $\nu[fp]\otimes\pi g_{9/2}\otimes\pi g_{9/2}$ and $\nu g_{9/2}\otimes\pi g_{9/2}\otimes\pi g_{9/2}$, respectively. Perhaps the multitude of states observed in ^{77}Se arises from the different combinations of Nilsson orbitals available. Deformed shell-model calculations in the Br isotopes [26] have shown that one specific configuration usually lies lower in energy, but perhaps a near degeneracy occurs in ^{77}Se.

V. SUMMARY

High-spin states in ^{77}Se were populated using the ^{76}Ge $(\alpha,3n)$ reaction and their γ decays were observed with the Pitt-FSU detector array. The positive-parity yrast structure was extended up to the 6655 keV $(\frac{31}{2}^+)$ level and the lowest negative-parity band was extended up to the 5583 keV $(\frac{27}{2}^-)$ level. Spin assignments were made using the measured DCO ratios.

This work clarifies how the structure of ^{77}Se compares with that of the heavier $N=43$ isotones ^{79}Kr, ^{81}Sr, and ^{83}Zr. A strong similarity was seen in the positive-parity yrast band. The large signature splitting present at low spins almost vanishes above the first band crossing at a rotational

frequency of $\hbar\omega \approx 0.5$ MeV. Theoretically, the character of the band changes because of a change in shape driven by the pair of aligned $g_{9/2}$ quasiprotons. Two other positive-parity structures in ^{77}Se built on $\frac{5}{2}^+$ and $\frac{11}{2}^+$ bandheads also have close analogs in the heavier isotones.

The $\frac{1}{2}^-$ ground-state band and the more strongly populated $\frac{5}{2}^-$ band in ^{77}Se show many similarities with the corresponding bands in the heavier isotones. The very weak $M1$ transitions in the $\frac{5}{2}^-$ band appear to result from a near cancellation between the magnetic moments due to collective rotation and to the $[303]\frac{5}{2}$ neutron. The opposite sign of the signature splitting between the $\frac{1}{2}^-$ and $\frac{5}{2}^-$ bands is probably due to differences in the triaxiality shape parameter γ for these well-deformed ($\beta_2 \approx 0.29$) bands.

A complex of negative-parity states with $I \geq \frac{15}{2}$ and $E_x \geq 2.8$ MeV was observed in ^{77}Se. Such a complex feature is unique among the $N=43$ isotones and nearby f-p-g shell nuclei, although single decay sequences of mainly $\Delta I = 1$ transitions have been reported in ^{79}Kr and a number of odd-Z nuclei. The states may be based on 3qp configurations of the general form $\pi[fp] \otimes \pi g_{9/2} \otimes \nu g_{9/2}$ involving noncollective rotation of an oblate shape.

ACKNOWLEDGMENTS

We are grateful to J.X. Saladin whose loan of the University of Pittsburgh detectors and electronics made the combined Pitt-FSU detector array possible. We are also grateful to E.G. Myers who developed the α source and to P.B. Semmes and I. Ragnarsson who provided the particle-rotor codes. This work was supported in part by the National Science Foundation.

[1] E.F. Moore, P.D. Cottle, C.J. Gross, D.M. Headly, U.J. Hüttmeier, S.L. Tabor, and W. Nazarewicz, Phys. Rev. C **38**, 696 (1988); Phys. Lett. B **211**, 14 (1988).

[2] F. Cristancho, D.R. LaFosse, C. Baktash, D.F. Winchell, B. Cederwall, J. Döring, C.J. Gross, P.-F. Hua, H.-Q. Jin, M. Korolija, E. Landulfo, I.Y. Lee, A.O. Macchiavelli, M.R. Maier, W. Rathbun, J.X. Saladin, D. Sarantites, D.W. Stracener, S.L. Tabor, A. Vander Mollen, and T.R. Werner, Phys. Lett. B **357**, 281 (1995).

[3] F. Lidén, J. Billowes, C. Mort, B.J. Varley, W. Gelletly, C.J. Gross, and D.D. Warner, Daresbury Annual Report 1993, p. 7.

[4] S.E. Arnell, C. Ekström, L.P. Ekström, A. Nilsson, I. Ragnarsson, P.J. Smith, and E. Wallander, J. Phys. G **9**, 1217 (1983).

[5] R. Schwengner, J. Döring, L. Funke, G. Winter, A. Johnson, and W. Nazarewicz, Nucl. Phys. **A509**, 550 (1990).

[6] G.D. Johns, J. Döring, J.W. Holcomb, T.D. Johnson, M.A. Riley, G.N. Sylvan, P.C. Womble, V.A. Wood, and S.L. Tabor, Phys. Rev. C **50**, 2786 (1994).

[7] M. Behar, A. Filevich, A.O. Macchiavelli, L. Szybisz, and P. Thieberger, Phys. Rev. C **26**, 1417 (1982).

[8] U.J. Hüttmeier, C.J. Gross, D.M. Headly, E.F. Moore, S.L. Tabor, T.M. Cormier, P.M. Stwertka, and W. Nazarewicz, Phys. Rev. C **37**, 118 (1988).

[9] D. Rudolph, C.J. Gross, K.P. Lieb, W. Gelletly, M.A. Bentley, H.G. Price, J. Simpson, B.J. Varley, J.L. Durell, Ö. Skeppstedt, and S. Rastikerdar, Z. Phys. A **338**, 139 (1991).

[10] S. Suematsu, Y. Haruta, B.J. Min, K. Heiguchi, Y. Ishikawa, S. Mitarai, T. Kuroyanagi, and Y. Onizuka, Nucl. Phys. **A485**, 304 (1988).

[11] W. Fieber, K. Bharuth-Ram, J. Heese, F. Cristancho, C.J. Gross, K.P. Lieb, S. Skoda, and J. Eberth, Z. Phys. A **332**, 363 (1989).

[12] K.O. Zell, H.-G. Friederichs, B. Heits, D. Hippe, H.W. Schuh, P. von Brentano, and C. Protop, Z. Phys. A **276**, 371 (1976).

[13] M. Honusek, A. Špalek, J. Adam, P. Tlustý, J. Döring, L. Funke, R. Schwengner, and G. Winter, Rossendorf Annual Report 1988, ZfK-667, 1989, p. 27.

[14] Y. Tokunaga, H. Seyfarth, R.A. Meyer, O.W.B. Schult, H.G. Börner, G. Barreau, H.R. Faust, K. Schreckenbach, S. Brant, V. Paar, M. Vouk, and D. Vretenar, Nucl. Phys. **A439**, 427 (1985).

[15] Y.G. Kosyak and L.V. Chekushina, Izv. Akad. Nauk SSSR, Ser. Fiz. **55**, 2187 (1991).

[16] M.F. Kudoyarov, E.V. Kuzmin, A.A. Pasternak, J. Adam, M. Honusek, and A. Špalek, in Proceedings of the Annual Conference on Nuclear Spectroscopy and Structure of Atomic Nuclei, Leningrad, 1990 (unpublished), pp. 59 and 61.

[17] S.L. Tabor and J. Döring, Phys. Scr. **T56**, 175 (1995).

[18] S.L. Tabor, M.A. Riley, J. Döring, P.D. Cottle, R. Books, T. Glasmacher, J.W. Holcomb, J. Hutchins, G.D. Johns, T.D. Johnson, T. Petters, O. Tekyi-Mensah, P.C. Womble, L. Wright, and J.X. Saladin, Nucl. Instrum. Methods Phys. Res. B **79**, 821 (1993).

[19] S.L. Tabor, Nucl. Instrum. Methods Phys. Res. A **265**, 495 (1988).

[20] W. Nazarewicz, J. Dudek, R. Bengtsson, T. Bengtsson, and I. Ragnarsson, Nucl. Phys. **A435**, 397 (1985).

[21] S.E. Larsson, G. Leander, and I. Ragnarsson, Nucl. Phys. **A307**, 189 (1978).

[22] Paul. B. Semmes and Ingemar Ragnarsson, in *High Spin Physics and Gamma-Soft Nuclei*, edited by J.X. Saladin, R.A. Sorensen, and C.M. Vincent (World Scientific, Singapore, 1991), p. 500.

[23] T. Bengtsson and I. Ragnarsson, Nucl. Phys. **A436**, 14 (1985).

[24] J.H. Hamilton, A.V. Ramayya, W.T. Pinkston, R.M. Ronningen, G. García-Bermúdez, H.K. Carter, R.L. Robinson, H.J. Kim, and R.O. Sayer, Phys. Rev. Lett. **32**, 239 (1974).

[25] S.L. Tabor, Phys. Rev. C **45**, 242 (1992).

[26] R. Sahu and S.P. Pandya, Nucl. Phys. **A529**, 20 (1991).